Nonlinear modeling of flexible manipulators using non-dimensional variables

M. Chandra Shaker[+], Ashitava Ghosal[*]

Abstract

This paper deals with nonlinear modeling of planar one and two link, flexible manipulators with rotary joints using finite element method (FEM) based approaches. The equations of motion are derived taking into account the non-linear strain-displacement relationship and two characteristic velocities, U_a and U_g, representing material and geometric properties (also axial and flexural stiffness), are used to non-dimensionalise the equations of motion. The effect of variation of U_a and U_g on the dynamics of planar flexible manipulator is brought out using numerical simulations. It is shown that above a certain U_g value (approximately ≥ 45 m/sec), a linear model (using linear strain-displacement relationship) and the non-linear model give approximately same tip deflection. Likewise it was found that the effect of U_a is prominent only if U_g is small. The natural frequencies are seen to be varying in a nonlinear manner with U_a and in a linear manner with U_g.

Keywords: Nonlinear model, flexible manipulators, non-dimensional equations, system mode

1   Introduction

Dynamic analysis of high-speed mechanisms, flexible manipulators and structures have received considerable attention in the past two decades. Most of the researchers, however, assume small deformation and use a linear strain-displacement relationship (see, for example, [1] - [8]). When accurate mathematical models are required, non-linear elastic deformation in structures may have to be considered. Non-linearities can arise out of non-linear elastic, plastic and visco-elastic behavior or there can be geometric non-linearities arising out of large deformations. In this paper, we deal only with geometric non-linearities.

[*]Corresponding author
Dept. of Mechanical Engineering, Indian Institute of Science, Bangalore 560 012, India
email: asitava@mecheng.iisc.ernet.in
+ Senior Software Engineer, Delmia Solution Pvt. Ltd., Bangalore,
email: chandrashaker_mulinti@delmia.com

When there are large deformations, it is more appropriate to use a non-linear strain-displacement relationship for the material. The use of non-linear strain-displacement relationship leads to the coupling between axial and bending modes of vibration. This fact is reported in several textbooks (see for example [9]), but has been applied to modeling of flexible manipulators by very few researchers. Bakr and Shabana [10] and Gordaninejad et al.[11] take into account geometric non-linearity and shear deformation in non-linear modeling of flexible systems. Simo and Vu-Quoc [13] showed that for rotating structures, the appropriate accounting of the influence of centrifugal force on the bending stiffness requires the use of a geometrically non-linear beam theory, and the use of a first order(linearized) linear beam theory results in a spurious loss of bending stiffness. Damaran and Sharf [12] have presented and classified the inertial and geometric non-linearities that arise in the motion and constraint equations for multi-body systems. They observed that for sufficiently fast maneuvers of flexible links of the manipulators, the linear beam theory approximation is completely inadequate. Mayo and Shabana [14] developed equations of motion of flexible multi-body systems retaining up to second order terms in the strain-displacement relationship. Shabana and co-workers [14, 15] show that consideration of longitudinal displacement caused by the bending would eliminate the third and higher order terms from the strain energy expression if strain energy is written in terms of axial deformation. This leads to non-linear inertia terms and a constant stiffness matrix. Du and Ling [16] have developed a general non-linear finite element model for dynamic analysis of three dimensional beam-like mechanisms undergoing both large rigid body motion and large elastic deflections. They adopted the non-linear strain-displacement relationship taking into account the axial strain and the shear strains due to the pre-twist in the beams. Al-Bedoor and Hamdan [17] used an assumed mode based non-linear dynamic model to study a rotating flexible arm. The link is, however, assumed to be inextensible and hence the geometric non-linearity arises out of the coupling between longitudinal displacement caused by bending and the transverse deflection of the link.

In this paper, we present finite element based models for planar one and two link flexible manipulators assuming that there are no dissipation and gravity effects. We use a nonlinear strain-displacement relationship to obtain the potential energy. The transverse shear and rotary inertia effects are neglected as the links are assumed to be long and slender. The equations of motion, obtained using the Lagrangian formulation, have been non-dimensionalised using two characteristic velocities, namely U_a the velocity of sound in the material, and U_g a characteristic velocity associated with bending. One of the main contribution of this paper is the study of the effect of variation of U_a and U_g on the tip displacement of a flexible one-link manipulator with a rotary(R) joint. It is shown that only below a certain U_g (approximately ≤ 45 m/sec), the geometric non-linearities begin to take effect and above this value of U_g, there is little difference between the results obtained from linear and non-linear models. The natural frequencies are seen to be varying in a non-linear way with U_a and in a linear fashion with U_g. We also present a FEM model of a two link flexible manipulator using the system mode approach ([18] - [21]) wherein it is assumed that a multi-link flexible manipulator or a structure vibrates with global or system mode characteristics rather than

2

a series of subsystem or component modes. On comparing the numerical results obtained from a system mode model and the commonly used component mode approach, it is observed that as the links of multi-link manipulators become more and more flexible, the component mode method of modeling shows greater deviation from the system mode method. However, for larger U_g, there is very little difference in terms of joint rotation and tip displacement between component and system mode formulations with lesser number of elements, and since the computational time for system mode formulations with lesser number of elements are smaller, the system mode formulations can be used to obtain dynamic behavior more efficiently.

This paper is organized as follows: in section 2, we present the nonlinear strain-displacement relationship used in the paper and the shape functions of the planar beam element taking into account flexural and axial deformation. In section 3, we present an FEM based non-linear modeling of a planar 1R kinked manipulator, and an algorithm to non-dimensionalise the equations of motion. In section 4, the approach of section 3 is extended to multi-link planar flexible manipulators with emphasis on a 2R flexible manipulator. In section 5, numerical simulation results for various models are presented and discussed, and in section 6, we present the conclusions.

2   Nonlinear strain-displacement relationship and shape functions

When the elastic displacements are small, a linear relationship is assumed between strain and displacements. However, if the displacements are large enough, nonlinear strain-displacement relations have to be used. For in-plane bending of beams, only the normal strain ϵ_{xx} need to be considered, and the full nonlinear strain-displacement relationship for ϵ_{xx} (assuming a 2D problem) is given as

$$\epsilon_{xx} = \frac{\partial u_x^*}{\partial x} + \frac{1}{2}\left[\left(\frac{\partial u_x^*}{\partial x}\right)^2 + \left(\frac{\partial u_y^*}{\partial x}\right)^2\right] \tag{1}$$

For small strain, $(\frac{\partial u_x^*}{\partial x})^2$ can be ignored in comparison to $\frac{\partial u_x^*}{\partial x}$, and we get

$$\epsilon_{xx} = \frac{\partial u_x^*}{\partial x} + \frac{1}{2}\left(\frac{\partial u_y^*}{\partial x}\right)^2 \tag{2}$$

where the variables u_y^*, u_x^* denote the field displacement variables defined over the entire domain. Further, from classical beam theory, we can write

$$\epsilon_{xx} = \frac{\partial u_x}{\partial x} - y\frac{\partial^2 u_y}{\partial x^2} + \frac{1}{2}\left(\frac{\partial u_y}{\partial x}\right)^2 \tag{3}$$

where y is measured from the neutral axis of the beam and u_x, u_y denotes the longitudinal and transverse displacement, respectively, at $y = 0$[9]. This is the *nonlinear strain-displacement relationship* that has been used in this paper for nonlinear modeling.

Assuming a *linear* stress-strain relationship, the potential energy can be obtained as

$$U = \frac{E}{2} \int_v \epsilon_{xx}^2 dV$$

Expanding the above integral, and since y is measured from the neutral axis, all integrals of the form $\int y \, dA$ must vanish, we get

$$U = \frac{EA}{2} \int_0^l \left(\frac{\partial u_x}{\partial x}\right)^2 dx + \frac{EI}{2} \int_0^l \left(\frac{\partial^2 u_y}{\partial x^2}\right)^2 dx + \frac{EA}{2} \int_0^l \left(\frac{\partial u_x}{\partial x}\right) \left(\frac{\partial u_y}{\partial x}\right)^2 dx + \frac{EA}{2} \int_0^l \frac{1}{4} \left(\frac{\partial u_y}{\partial x}\right)^4 dx \tag{4}$$

where E, A, I and l denote the Young's modulus, cross-sectional area, moment of inertia of the cross-section and length respectively, and in this paper, A and I are assumed to be constant.

In this paper, the flexural and axial deformations of the links are approximated using the finite element method. Each flexible link is assumed to be discretised into a finite number of beam elements, with each element consisting of two nodes with three degrees of freedom at each node. For the assumed nodal displacements and rotations, the displacement of any arbitrary point in the element can be expressed as [9],

$$\left\{ \begin{array}{c} u_{x_i} \\ u_{y_i} \end{array} \right\} = \left[\begin{array}{cccccc} N_1 & 0 & 0 & N_4 & 0 & 0 \\ 0 & N_8 & N_9 & 0 & N_{11} & N_{12} \end{array} \right] \{q_i\}^T \tag{5}$$

where the shape functions, N_i's, are given by

$$\begin{aligned} N_1 &= 1 - \xi, \quad N_4 = \xi \\ N_8 &= 1 - 3\xi^2 + 2\xi^3, \quad N_9 = \left(\xi - 2\xi^2 + \xi^3\right) l \\ N_{11} &= 3\xi^2 - 2\xi^3, \quad N_{12} = \left(-\xi^2 + \xi^3\right) l \\ \xi &= \frac{x}{l} \end{aligned}$$

The quantities u_{x_i} and u_{y_i} are the displacements of any arbitrary point of the ith element along the X-axis and Y-axis respectively. The vector of nodal degrees of freedom of the ith beam element (see figure 1) is given by

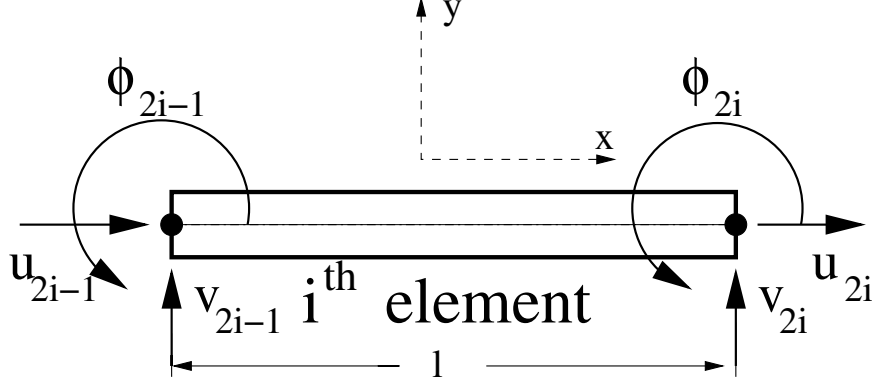$$\{q_i\} = \{u_{2i-1}, v_{2i-1}, \phi_{2i-1}, u_{2i}, v_{2i}, \phi_{2i}\}$$

4

Figure 1: Planar beam element

3 Finite element model of 1R planar kinked manipulator

We start by modeling a general 1R planar kinked manipulator shown in figure 2. The use of the kinked manipulator model allows us to obtain a FEM based *system mode model*[18] for a planar 2R flexible manipulator as shown in section 4. Unlike the conventional way of modeling a single link flexible manipulator[6, 8], a slightly different approach has been used to model the 1R kinked manipulator (Please see Appendix B for a comparison of the proposed model and the conventional model). In our approach, a local co-ordinate system is defined for each element of the link as shown in figure 2. In figure 2, OXY is the global co-ordinate system and $O_iX_iY_i$ is the body fixed co-ordinate system with O_iX_i along the tangent at the $(2i-2)^{\text{th}}$ node of the system. The co-ordinate system $O_kX_kY_k$ is the body fixed frame at the kink with O_kX_k along the tangent to the deformed configuration of the link at the $(2n_k)^{\text{th}}$ node. The position vector of a point in an arbitrary i^{th} element is obtained by appropriately considering the position vector of the corresponding local origin in the global co-ordinate system. We get

$$
{}^0_i\mathbf{P} = {}^0_{i-1}\mathbf{P}\bigg|_{x=l_{i-1}} + [R_\psi]\left\{ \begin{array}{c} x + u_{x_i} \\ u_{y_i} \end{array} \right\} \qquad 0 \le x \le l_i \qquad (6)
$$

$$
[R_\psi] = \left[\begin{array}{cc} \cos\psi & -\sin\psi \\ \sin\psi & \cos\psi \end{array} \right]
$$

$$
\text{for} \qquad 1 \le i \le n_k \qquad \psi = \theta_1 + \sum_{j=1}^{i} \phi_{2j-2}
$$

$$
\text{for} \qquad n_k < i \le N \qquad \psi = \theta_1 + \sum_{j=1}^{i} \phi_{2j-2} + \delta
$$

5

where $(u_{x_i}, u_{y_i})^T$ is given by equation (5), n_k is the number of elements before the kink and N is the *total* number of elements in the kinked manipulator. In the above equation $[R_\psi]$ is the transformation matrix from local element co-ordinate system to global inertial frame. For a zero kink angle, i.e., for a single link 1R planar manipulator, equation (6) becomes

$$
{}^0_i\mathbf{P} = {}^0_{i-1}\mathbf{P}\bigg|_{x=l_{i-1}} + [R_\psi] \left\{ \begin{array}{c} x + u_{x_i} \\ u_{y_i} \end{array} \right\} \qquad 0 \le x \le l_i, \quad \psi = \theta_1 + \sum_{j=1}^{i} \phi_{2j-2} \qquad (7)
$$

It must be noted that, in the proposed method, the co-ordinate transformation from the element frame to global frame is dynamic due to the presence of $[R_\psi]$, where ψ is a function of time dependent nodal rotations. As a result the position vector of an arbitrary point in the link is a nonlinear function of nodal rotations. The expressions for the position vector of the far end of a single link planar manipulator modeled with the proposed technique and the conventional method is presented in Appendix B.
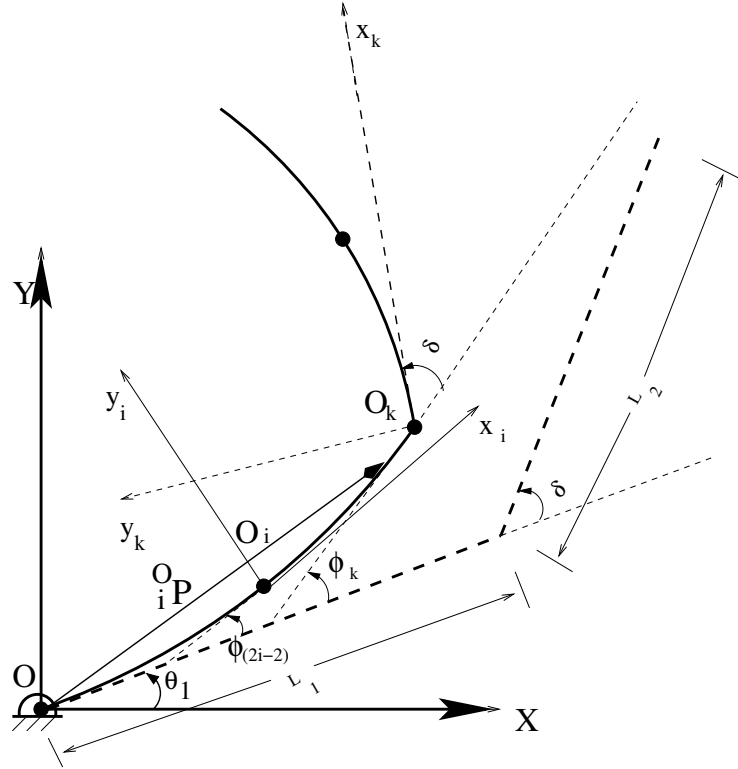

Figure 2: Modeling of a 1R kinked planar manipulator(proposed method)

3.1   Expression for kinetic energy

Once the position vector of an arbitrary point on the ith element, ${}^0_i\mathbf{P}$, is known, we can obtain the velocity of the point in the fixed co-ordinate system. The kinetic energy of the

6

kinked beam is the summation of kinetic energies of each individual element obtained using appropriate velocity vectors. The kinetic energy of ith element is given by

$$K.E_i = \frac{1}{2} \int_0^{l_i} \rho_i A_i \left[\frac{d_i^0 \mathbf{P}}{dt} \right]^T \frac{d_i^0 \mathbf{P}}{dt} \, dx \quad 1 \leq i \leq N \tag{8}$$

The total kinetic energy of the link is given by

$$T = \sum_{i=1}^{N} K.E_i = \frac{1}{2} \dot{Q}^T [M] \dot{Q} \tag{9}$$

where the generalized co-ordinates, Q, is given by $\{\theta_1, S\}^T$ – the vector of nodal variables of all the elements denoted by S is $\{u_1, v_1, \phi_1, \cdots, u_{2N}, v_{2N}, \phi_{2N}\}$, θ_1 is the rigid rotation at the joint, and $[M]$ is the mass matrix.

3.2 Expression for potential energy

As given in equation (4), the potential energy for each individual element of the kinked beam is given by

$$
\begin{aligned}
U_i \;=\; & \frac{E_i A_i}{2} \int_0^{l_i} \left(\frac{\partial u_{x_i}}{\partial x} \right)^2 dx + \frac{E_i I_i}{2} \int_0^{l_i} \left(\frac{\partial^2 u_{y_i}}{\partial x^2} \right)^2 dx \\
& + \frac{E_i A_i}{2} \int_0^{l_i} \left(\frac{\partial u_{x_i}}{\partial x} \right) \left(\frac{\partial u_{y_i}}{\partial x} \right)^2 dx + \frac{E_i A_i}{2} \int_0^{l_i} \frac{1}{4} \left(\frac{\partial u_{y_i}}{\partial x} \right)^4 dx
\end{aligned}
$$

The total potential energy of the system is given by

$$V = \sum_{i=1}^{N} U_i = \frac{1}{2} S^T \left([K] + [\Delta K(S)] \right) S \tag{10}$$

where $[K]$ is the conventional stiffness matrix and $[\Delta K(S)]$ is the geometric stiffness matrix.

3.3 Boundary and compatibility conditions

The joint has only rotational degree of freedom with respect to OX and the link length is very large compared to the hub diameter. Therefore, as per the conventional modeling, for *clamped boundary conditions*[1] we have the constraint

$$u_1 = 0, v_1 = 0, \phi_1 = 0 \tag{11}$$

---

[1]The choice of coordinate systems, mode of deformation, and the boundary conditions are linked[22], and *pinned* boundary conditions have also been used in literature for some applications.

In our approach, since each element of link is assumed to have its own local co-ordinate system, and we have

$$u_{2i-1} = 0, v_{2i-1} = 0, \phi_{2i-1} = 0 \quad \forall \quad 1 \leq i \leq N \tag{12}$$

It must be noted that, in the proposed technique $u_{2i-1}, v_{2i-1}, \phi_{2i-1}$ are local displacements and rotation in the ith co-ordinate system.

3.4 Equations of motion of 1R kinked planar manipulator

The equations of motion are derived using the Lagrangian formulation. The Lagrangian of the flexible system in terms of the generalized co-ordinates, Q, and its derivatives, $\dot{Q}$, is given by $L(Q, \dot{Q}) = T - V$, where T and V are total kinetic and potential energy of the system. From the Lagrange formulation, the equations of motion are obtained as

$$\frac{d}{dt} \left(\frac{\partial L\left(Q, \dot{Q}\right)}{\partial \dot{Q}_i} \right) - \frac{\partial L\left(Q, \dot{Q}\right)}{\partial Q_i} = \tau_i \tag{13}$$

The above equation in conjunction with the boundary and compatibility conditions, yields the dynamic equations of motion which can be written in a general form as

$$[M(Q)] \left\{ \ddot{Q} \right\} + \left([K] + [\Delta K(Q_f)] \right) \{Q_f\} + h(Q, \dot{Q}) = \tau \tag{14}$$

where $[M]$ is the system mass matrix, $[K]$ is the conventional stiffness matrix, $[\Delta K]$ is the geometric stiffness matrix, $h(Q, \dot{Q})$ is the vector of centripetal and Coriolis terms, τ is the vector $[\Gamma, 0, 0, \cdots, 0]^T$ with Γ as the vector of input torques at the joints, and Q_f is the vector of flexible variables. It may be noted that there are $(3N + 1)$ second order ordinary differential equations (N is the *total* number of elements in the kinked manipulator), which can be numerically integrated with given initial conditions and external torque at the joint.

3.5 Non-dimensional equations of motion

The dynamic equations of motion derived above contain a large number of parameters, the variation of each of which affects the system behavior in a complex manner. Hence, to study the system behavior effectively and exhaustively, it would be advantageous if several parameters can be combined and the equations of motion can be non-dimensionalised. A possible algorithm for non-dimensionalisation of equations of motion is as follows:

- Divide all the equations throughout by $A_1 \rho_1 L_1$ present in the mass matrix.

- Introduce the parameters shown below

$$U_{g_1} = \frac{1}{L_1} \sqrt{\frac{E_1 I_1}{\rho_1 A_1}}, \quad U_{g_2} = \frac{1}{L_2} \sqrt{\frac{E_2 I_2}{\rho_2 A_2}}, \quad U_{a_1} = \sqrt{\frac{E_1}{\rho_1}}, \quad U_{a_2} = \sqrt{\frac{E_2}{\rho_2}}$$

$$\mathcal{T} = t/(L_1/U_{g_1}), \quad m = \frac{\rho_2 A_2}{\rho_1 A_1}, \quad L = \frac{L_2}{L_1} \tag{15}$$

It may be noted that U_a is the speed of sound in the material and U_g with units of meters per second is a characteristic velocity associated with bending vibration. The quantity U_g is motivated from the 1D beam equation

$$\frac{EI}{\rho A}\frac{\partial^4 \phi}{\partial x^4} + \frac{\partial^2 \phi}{\partial t^2} = 0$$

by recognizing the fact that dividing $\sqrt{\frac{EI}{\rho A}}$ by the length L will yield a quantity with units of meters/sec[23]. It can be seen that U_g is dependent on the geometry and material properties of the beam where as U_a is purely a material property. It can also be seen that U_a is related to axial stiffness where as U_g is related to the flexural rigidity EI and also depends on L. It must be kept in mind that the velocities U_a and U_g are for the *linear* system, and $U_{g_i}, U_{a_i}, \ i = 1, 2$ are the velocities associated with the part of kinked beam with length $L_i \ i = 1, 2$. The symbol $\mathcal{T}$ denotes the non-dimensional time variable.

- Replace all the first and second derivatives with respect to t by first and second derivatives with respect to $\mathcal{T}$ by using chain rule. We get

$$\begin{aligned}
\dot{Q} &= \frac{dQ}{d\mathcal{T}} \cdot \frac{d\mathcal{T}}{dt} = \left(\frac{U_{g_1}}{L_1}\right) Q' \\
\ddot{Q} &= \left(\frac{U_{g_1}}{L_1}\right)^2 Q''
\end{aligned} \tag{16}$$

- Replace the nodal variables (u_i, v_i) by non-dimensional nodal variables (U_i, V_i) defined by

$$U_i = \frac{u_i}{L_1}, \quad V_i = \frac{v_i}{L_1}$$

- After making few simplifications and dividing throughout by $U_{g_1}^2$, we obtain the non-dimensional form of the equations of motion as

$$[\mathcal{M}(\mathcal{Q}_f)]\{\mathcal{Q}''\} + \{\mathcal{H}(\mathcal{Q}, \mathcal{Q}')\} + \left(\mathcal{K} + \Delta\mathcal{K}\left(\mathcal{Q}_f, \frac{U_{g_2}}{U_{g_1}}, \frac{U_{a_1}}{U_{g_1}}, \frac{U_{a_2}}{U_{g_1}}\right)\right)\{\mathcal{Q}\}$$

$$= \frac{\tau}{(A_1\rho_1 L_1) U_{g_1}^2} \tag{17}$$

where $(\cdot)', (\cdot)''$ represents the first and second derivatives with respect to non-dimensional time $\mathcal{T}$, $\mathcal{M}$ is the non-dimensional mass matrix, $\mathcal{K}$ and $\Delta\mathcal{K}$ are the non-dimensional conventional stiffness matrix and the geometric stiffness matrix respectively, and $\mathcal{H}$ is the vector of non-dimensional centripetal and Coriolis terms. The mass and stiffness matrices of the system in the non-dimensionalised form are shown in Appendix A.

4 System mode modeling of multi-link manipulators

It has been argued that, at resonant frequencies, a complex structure vibrates with *system mode* characteristics, rather than a series of *component modes* [20]. We derive the dynamic equations of motion of a planar 2R flexible manipulator modeled using the *finite element based, system mode method* and compare it with the component mode method of modeling. The formulation of equations of motion of a 2R planar manipulator using the system mode method involves the assumption that at each instant of time, during its motion, the second joint is *locked* so that the manipulator behaves as a single kinked beam with varying kink angle. For the rigid kinetic energy, however, it is assumed that the second joint is unlocked. Figure 2 also represents a 2R planar manipulator with δ and θ_2 representing the second joint angle. The position vector of any arbitrary point in the ith element of the kinked link is given by

For $\quad 1 \leq i \leq n_k$

$$\left.{}^O_i\mathbf{P} = {}^O_{i-1}\mathbf{P}\right|_{x=l_{i-1}} + [R_\psi]\left\{\begin{array}{c} x + u_{x_i} \\ u_{y_i} \end{array}\right\} \qquad \psi = \theta_1 + \sum_{j=1}^i \phi_{2j-2}\,, \quad 0 \leq x \leq l_i \qquad (18)$$

For $\quad n_k < i \leq N$

$$\left.{}^O_i\mathbf{P} = {}^O_{i-1}\mathbf{P}\right|_{x=l_{i-1}} + [R_\beta]\left\{\begin{array}{c} x \\ 0 \end{array}\right\} + [R_\psi]\left\{\begin{array}{c} u_{x_i} \\ u_{y_i} \end{array}\right\} \qquad\qquad 0 \leq x \leq l_i \qquad (19)$$

$$\beta = \theta_1 + \sum_{j=1}^i \phi_{2j-2} + \theta_2,\ \ \psi = \theta_1 + \sum_{j=1}^i \phi_{2j-2} + \delta$$

where $(u_{x_i}, u_{y_i})^T$ is given by the equation (5), n_k is the number of elements before the kink, N is the total number of elements in the kinked manipulator, and $[R_\psi]$ and $[R_\beta]$ are the transformation matrices from local element co-ordinate system to global inertial frame.

In the component mode method of modeling of 2R planar flexible manipulator, we define separate link co-ordinate systems for each link so that the position vector of an arbitrary point in a link is defined with respect to its link co-ordinate system.

4.1 The kinetic energy

The kinetic energy of the system is the summation of kinetic energies of each individual element of the kinked link. The total kinetic energy of the system is same as equation (9) but the generalized co-ordinates are $Q = \{\theta_1, \theta_2, S\}^T$, and the nodal degrees of freedom of all the elements are $S = \{u_1, v_1, \phi_1, \cdots, u_{2N}, v_{2N}, \phi_{2N}\}$. In the component mode method, the general matrix form of the kinetic energy remains similar to that in equation (9) with the total kinetic energy determined as the summation of kinetic energies of the two separate flexible links. The individual matrix elements will be different from those obtained from the system mode approach.

4.2 The potential energy

The potential energy of the 2R planar manipulator system is only due to the axial strain of the kinked link as the shear and torsional effects are neglected. The total potential energy of the system is same as equation (10) because the 2R planar manipulator is treated as a single link kinked manipulator vibrating with system modes. In the component mode approach, the total potential energy can be determined as the summation of the potential energies of the two flexible links due to the axial strain.

4.3 Boundary and compatibility conditions

Each element of the kinked link is assumed to have its own local co-ordinate system. Therefore, for *clamped boundary conditions*, we have

$$u_{2i-1} = 0, v_{2i-1} = 0, \phi_{2i-1} = 0 \quad \forall \quad 1 \le i \le N \tag{20}$$

In the component mode approach, for clamped boundary conditions, we have

$$u_1 = 0, v_1 = 0, \phi_1 = 0 \tag{21}$$

at the first node of *both* link 1 and link 2.

4.4 Equations of motion of 2R planar manipulator

The equations of motion of 2R planar flexible manipulator are derived along the same lines of 1R kinked planar manipulator except that, for the 2R case, the second joint rotation angle θ_2 also exists in addition to the kink angle δ. The general structure of the equations of motion of a 2R planar flexible manipulator remains the same as the equation (14). However, it may be noted that there are $3N + 2(N$ denotes the total number of elements of the kinked manipulator taken into consideration) second-order ordinary differential equations which need to be numerically integrated with given initial conditions and external torques at the joints. The above equations of motion can be non-dimensionalised using algorithm given in section 3.5.

In comparison, a component mode formulation of a 2R manipulator, with M elements in each link, the number of second-order ordinary differential equations would be $2(3M) + 2^2$. We show in the next section that for large U_g values, the system mode approach gives similar values of tip displacements, as compared to a component mode approach, with significantly less number of elements and, consequently, less number of ordinary differential equations. This results in significant reduction in computational time for numerical simulation.

---

[2]If M and N are same, then the number of second-order ordinary differential equations will be larger for the component mode approach.

5 Numerical simulations and results

In this section, we present the numerical simulation results of the mathematical models developed in the sections 3 and 4. Several simulations were performed for varying sinusoidal joint actuation torque, and we present a representative set of simulations. From these simulations, it is found that the tip deflection obtained from linear and nonlinear models are significantly different at low frequency actuation torques. Hence the nonlinear models are more relevant for low actuation frequencies. Further, a study of the effect of variation of U_a and U_g on the dynamics of 1R planar flexible manipulator revealed that the effect of axial rigidity shows up only at low flexural rigidities. The natural frequencies of vibration are seen to be varying non-linearly with U_a and in a linear fashion with U_g. Finally, a comparison of the simulation results of a 2R planar manipulator, modeled using finite element based component mode method and system mode method, shows that as the links of the 2R flexible manipulator become more and more flexible, the component mode method of modeling shows greater deviation from the system mode method.

The numerical simulations were performed on a COMPAQ XP1000 workstation. The ordinary second order differential equations of motion arising out of nonlinear modeling were solved using *ode23tb* which is a stiff differential equation solver in *Matlab*[24] – *ode23tb* is an implementation of TR-BDF2, an implicit Runge-Kutta formula with a trapezoidal rule first stage and a backward difference formula of order two in the second stage. It may be noted that all the simulations are performed using the non-dimensionalised equations of motion, however, some of the results are plotted with the dimensional form of the variables.

5.1 Dynamics of 1R planar kinked manipulator

We start with numerical simulation results of a 1R planar kinked manipulator with kink angle of 0 degrees. We compare the simulation results of linear and nonlinear models of 1R planar flexible manipulator developed using our approach (kinked beam method) and the conventional method. The simulations are performed assuming sinusoidal actuation torque at the joint. Figure 3 shows the plots of tip deflection of the 1R kinked planar manipulator for four models when the frequency of applied torque is low. Figure 4 shows the comparison of the four models for the case of a high frequency torque[3], and figure 5 shows tip deflections when the link has very high flexural rigidity ($EI = 4000 N-m^2$). We can make the following observations from these three figures:

- For the same number of elements in the link, it is clear from figure 3 that the linear kinked beam approach yields results much closer to that of the nonlinear models than the linear conventional approach.

- The difference between the conventional method(plots (a) and (c) in figure 3) and the proposed approach(plots (b) and (d) in figure 3) is due to the radial and tangential

---

[3]It may be noted that the chosen 'low' and 'high' actuation frequencies are much lower than the first natural frequency which is around 380 rad/sec.

inertial coupling effects present in the proposed approach. As explained in Appendix B, the proposed approach contains an extra term (see equations (22) and (23)) in the position vector. This difference leads to differences in the mass matrix derived by the two methods - in the proposed approach we get coupling between the radial and tangential inertial effects which is absent in the conventional method. The difference in the plots between the linear and nonlinear models is due to geometric stiffness.

- From figure 4, we can observe that all the four models give very close tip deflections and hence all models are good enough for modeling links when the applied torque is of high frequency.

- If the flexural stiffness of the link is very high, all the modeling methods are expected to show almost *identical* behavior and this is clearly seen in figure 5.

- It was observed that the contribution of fourth-order term in the potential energy expression (see section 3) toward tip deflection is very small and is of the order of 10^{-5}. Hence, in further simulations, the fourth-order term was not taken into account.

5.2 Effect of U_a and U_g

The equations of motion were non-dimensionalised by the use of two characteristic velocities, namely U_a and U_g. To study the effect of the characteristic velocities on the dynamics of flexible manipulators, we performed extensive numerical simulation for the 1R planar manipulator. The plot in figure 6(a) indicates the variation of maximum axial tip deflection for different materials, i.e., for different U_a values[4] with flexural rigidity and actuating torque remaining constant. The effect of variation of U_a is studied at two different values of flexural rigidity, i.e., two different U_g values[5] and actuation torque frequency. It can be observed that for a given U_g, the axial deflection is insensitive to actuation frequencies. However, the axial deflection at low frequency is higher compared to axial deflection at high actuation frequency, and, as expected, one can observe that the axial deflection increases when U_a decreases. To explain the variation of axial deflection with actuation frequency, we computed the joint angular velocity for $u_g = 25$ m/sec and $U_a = 4800$ m/sec. The maximum joint angular velocities, in non-dimensional units, were found to be about 0.6 and 0.0265 for low and high actuation frequency respectively. Hence, the higher axial tip deflection for low actuation frequency can be attributed to the larger centrifugal effects. Unlike the case of low frequency torque, there is almost no change in axial deflection with variation in U_a in the case of high frequency torque.

The plots in figure 6(b) shows the variation of maximum tip transverse deflection for different values of U_a with constant U_g and joint torque. It can be seen that for a link

---

[4]The range of the U_a values chosen, namely, from 1000 m/sec to 5000 m/sec represent plastic and steel respectively.

[5]It may be noted that for $\rho A = 0.1$ kg/m, and link length of 2 m, $U_g = 25$ m/sec represents $EI = 250$ $N - m^2$ and $U_g = 45$ m/sec represents $EI = 810 \ N - m^2$.
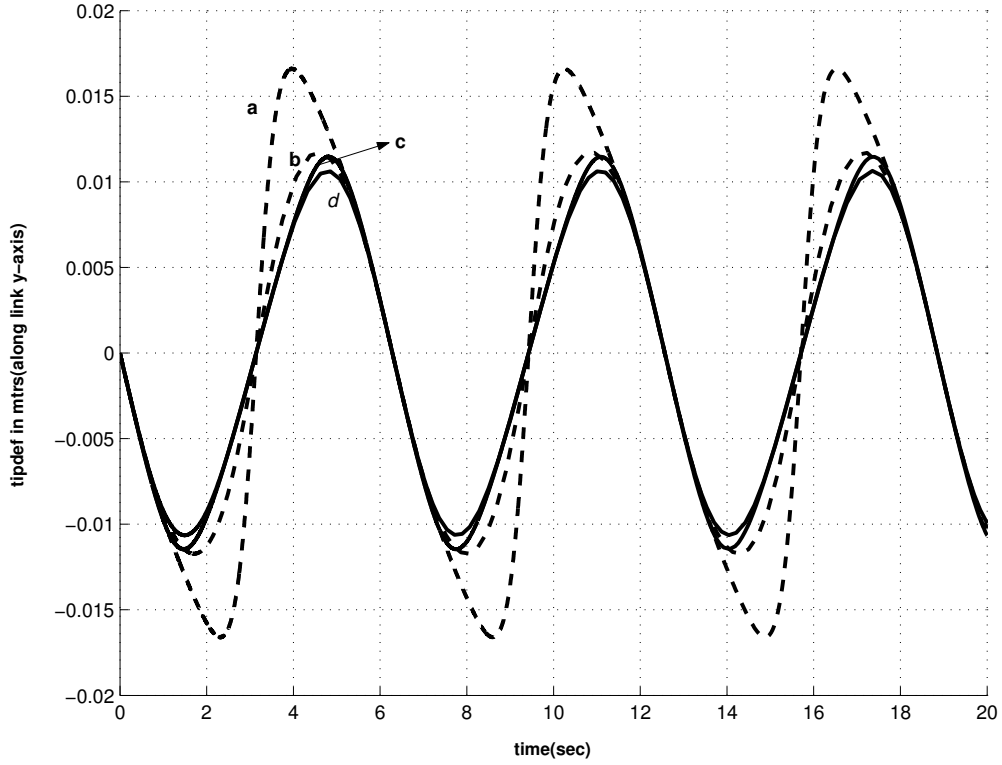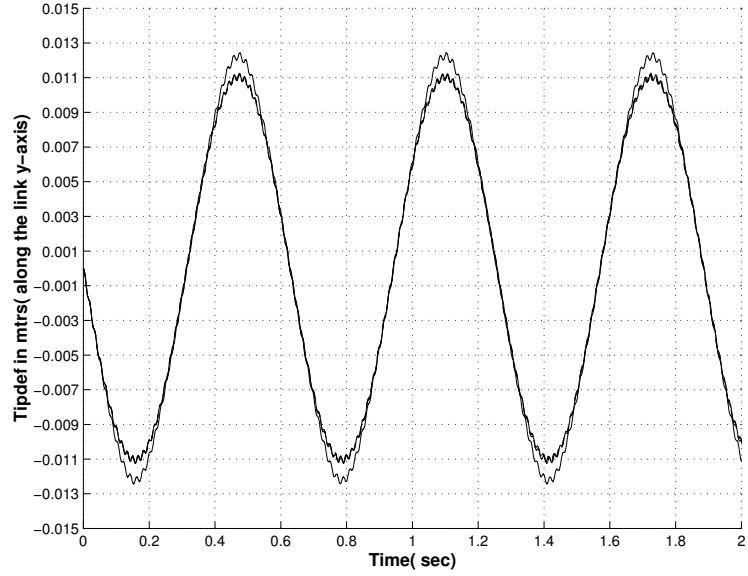
link length=2 m($L_1 = 1m$, $L_2 = 1m$), $U_g = 50m/sec$, $U_a = 4800m/sec$, $\rho A = 0.1kg/m$, $\delta = 0\deg$, $\tau_1 = 10\sin(1t)N - m$

(a) 1R planar linear conventional method   (c) 1R planar nonlinear conventional method

(b) 1R planar linear kinked beam method   (d) 1R planar nonlinear kinked beam method

Figure 3: Tip deflections of a 1R planar manipulator for a low frequency torque(4 models)

with high flexural rigidity (i.e., high U_g), the maximum tip transverse deflection is small and virtually there is no variation with change in U_a. When the link flexural rigidity is low, the variation of maximum tip transverse deflection with U_a is considerable. If the link is actuated with a high frequency torque the transverse tip deflections are large and increase with increase in U_a. However, the degree of the curve in case of high frequency torque appears to be greater than that of the low frequency torque.

In figure 7(a) and figure 7(b), we show the plot of maximum tip transverse deflection against U_g. The two plots indicate that as U_a decreases, the maximum tip deflection also decreases for any value of U_g. At high values($U_g \geq 45$ m/sec) of flexural rigidity the linear and non-linear models show almost the same maximum tip transverse deflection irrespective of the material properties(i.e, U_a). However, for a high and moderate frequency torques it is seen that the curves approach the linear model as U_a decreases. The trend of the curves is different for the case of low frequency torques as shown in the right-hand plot of figure 7. At high flexural rigidity values the linear model shows marginally higher maximum tip transverse deflection compared to the nonlinear models. However, as the link flexural rigidity

link length=2 m($L_1 = 1m$, $L_2 = 1m$), $U_g = 50m/sec$, $U_a = 4800m/sec$, $\rho A = 0.1kg/m$, $\delta = 0 \deg$, $\tau_1 = 10\sin(10t) \; N - m$
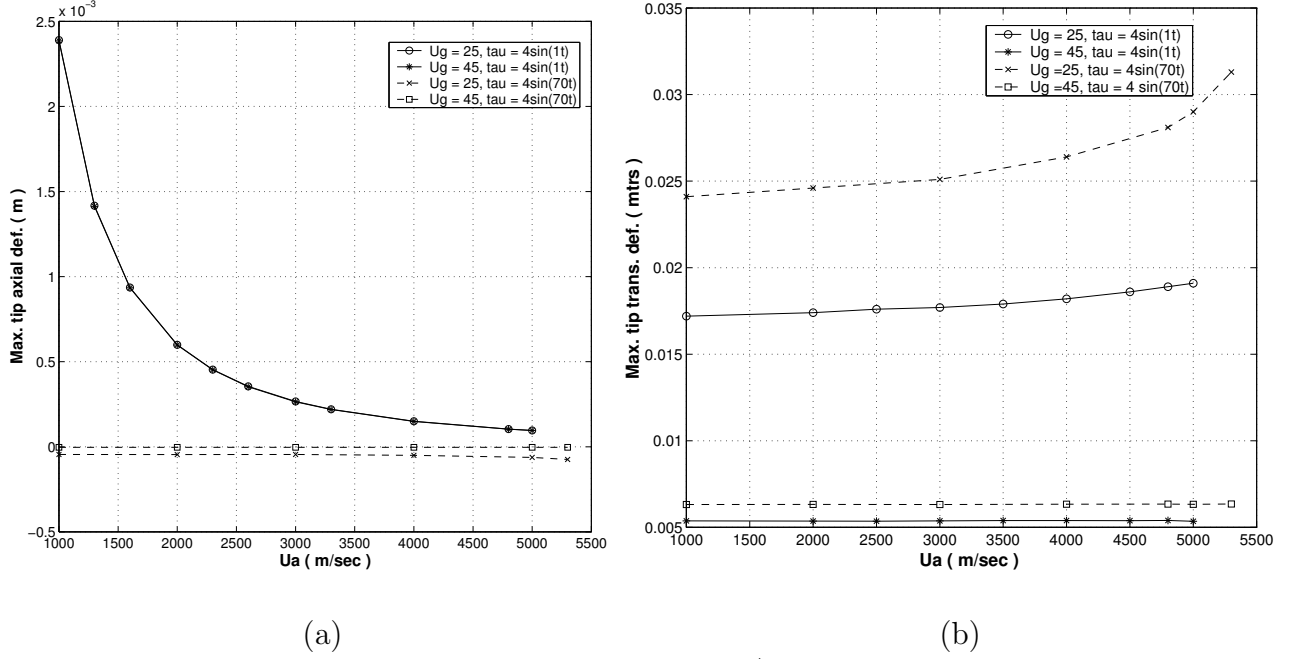
Figure 4: Tip deflection of a 1R planar manipulator for a high frequency torque(4 models)
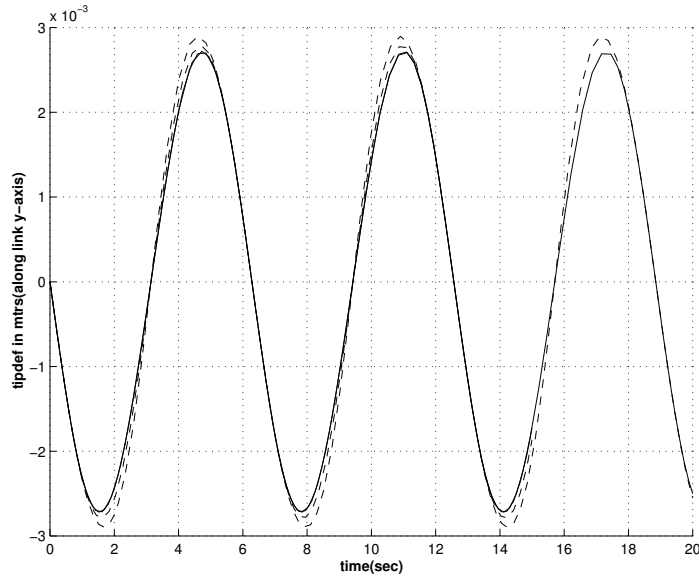
link length=2 m($L_1 = 1m$, $L_2 = 1m$), $U_g = 100m/sec$, $U_a = 4800m/sec$, $\rho A = 0.1kg/m$, $\delta = 0 \deg$, $\tau_1 = 10\sin(1t) \; N - m$

Figure 5: Tip deflection of a 1R planar manipulator with higher flexural rigidity(4 models)

decreases the non-linear models tend to exhibit higher maximum tip transverse deflection

15

<div align="center">(a)   (b)</div>

<div align="center">link length=2 m, $\rho A = 0.1 kg/m$, $\delta = 0 \deg$</div>

<div align="center">Figure 6: Plot of maximum tip axial and transverse deflection vs U_a</div>

than the linear model.

Figure 8 indicates the plot of first and second natural frequencies versus the time. It is seen that the natural frequency of the system does not remain constant with time but vary over a range of values. This may be attributed to the presence of geometric stiffness matrix which is a function of time. It can be observed that the variation of second natural frequencies with time is much larger than the first. Figure 9 shows a plot of the average(root mean square) value of the first natural frequency as a function of U_a. It can be seen that the first natural frequencies varies non-linearly with U_a. Figure 9 also shows a plot of the first natural frequency when a linear model (with $\Delta \mathcal{K} = 0$) is used. As expected the natural frequency does not change with time(and U_a) and we can also observe that the average natural frequency is larger than that obtained from a linear model. Figure 10(a) indicates the variation of fundamental frequency with respect to time for various U_g values. The fundamental frequency is seen to vary in a linear fashion with U_g as shown in figure 10(b), and does not vary significantly from the value obtained from a linear model with $\Delta \mathcal{K}$ as zero.

5.3 Effect of variation of kink angle on tip deflection

The equations of motion of the 1R kinked manipulator, modeled in section 3, are simulated to study the tip deflection at different kink angles. The linear and nonlinear models of the system are also compared for different kink angles.

<div align="center">16</div>
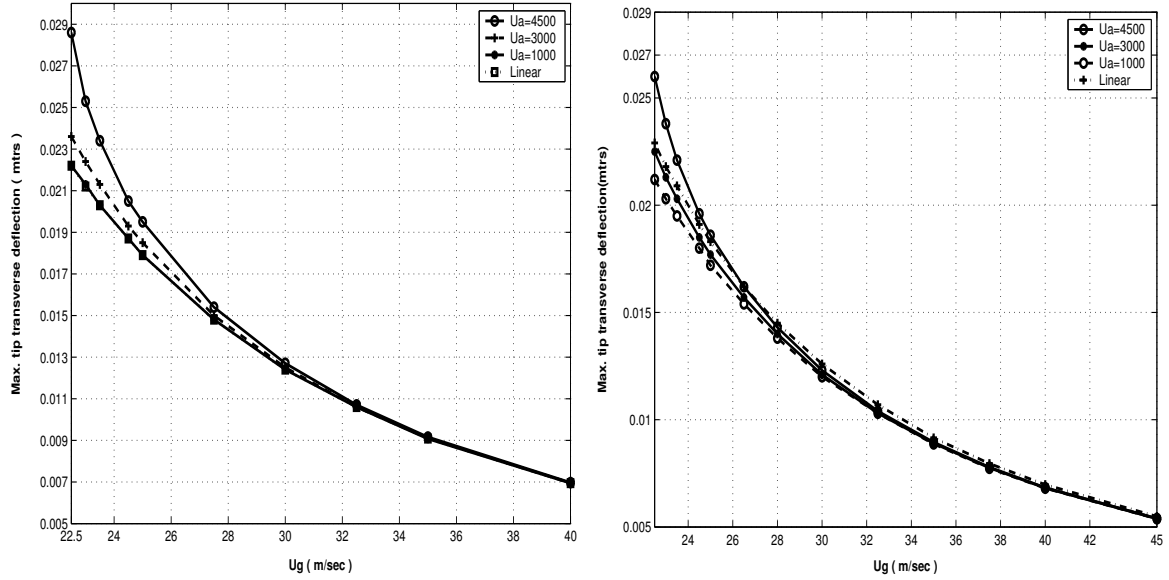
(a) $(\tau = 4\sin(5t))$ (b) $(\tau = 4\sin(1t))$
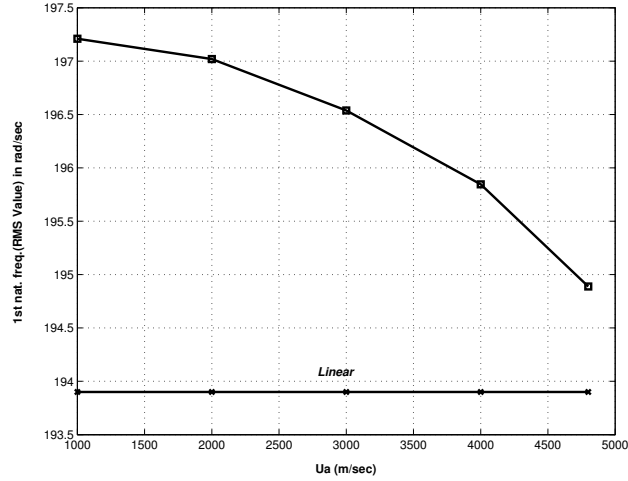
link length=2 m, $\rho A = 0.1 kg/m$, $\delta = 0 \deg$

Figure 7: Maximum tip transverse deflection for high and low frequency torque vs U_g
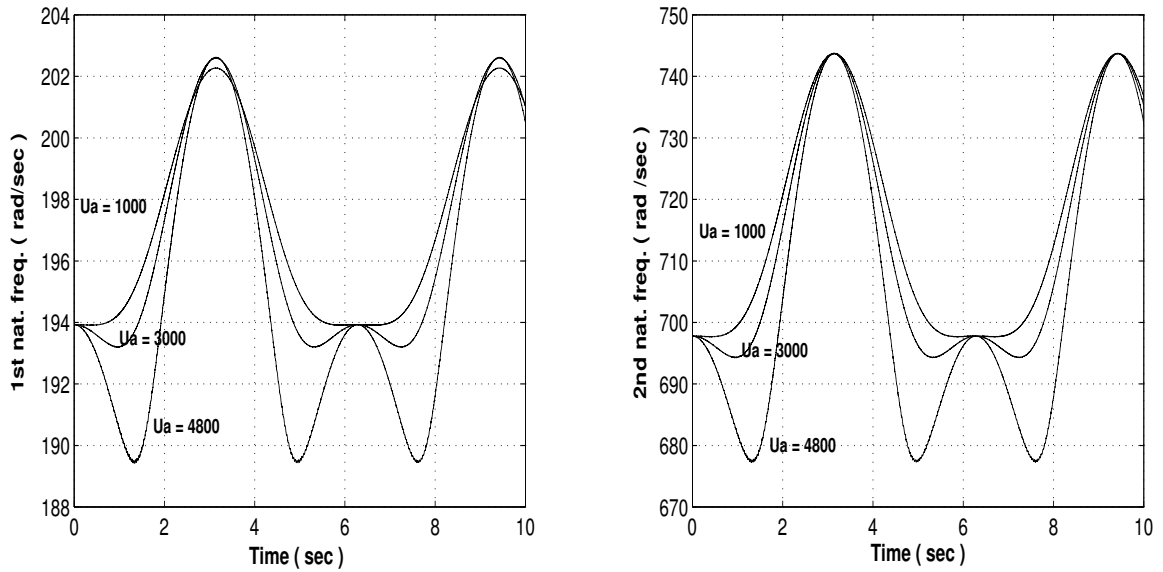
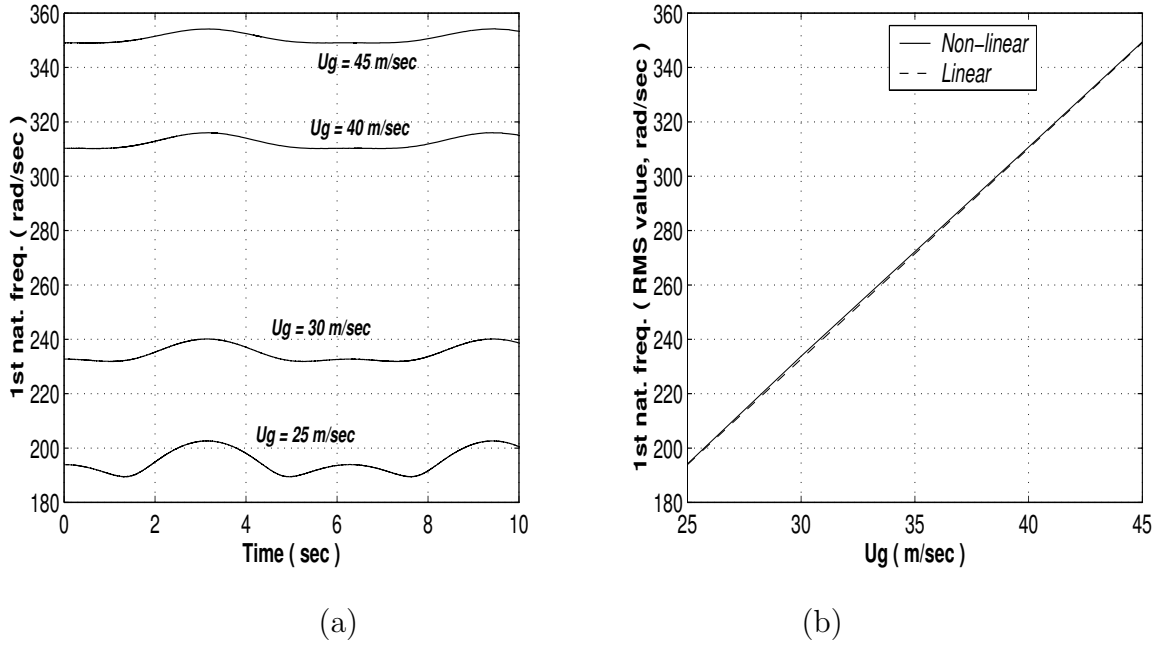link length=2 m, $\rho A = 0.1 kg/m$, $\tau = 5\sin(1t)$, $\delta = 0 \deg$, $U_g = 25 m/sec$

Figure 8: Plot of first and second natural frequencies vs time

Figure 11 indicates that the amplitude of tip deflection, along the Y-axis of the link co-ordinate system, decreases with increase in the kink angle. This is because the effective

17

link length=2 m, $\rho A = 0.1 kg/m$, $\tau = 5\sin(1t)$, $\delta = 0\deg$, $U_g = 25m/sec$

Figure 9: RMS average value of first natural frequency vs U_a

(a)   (b)
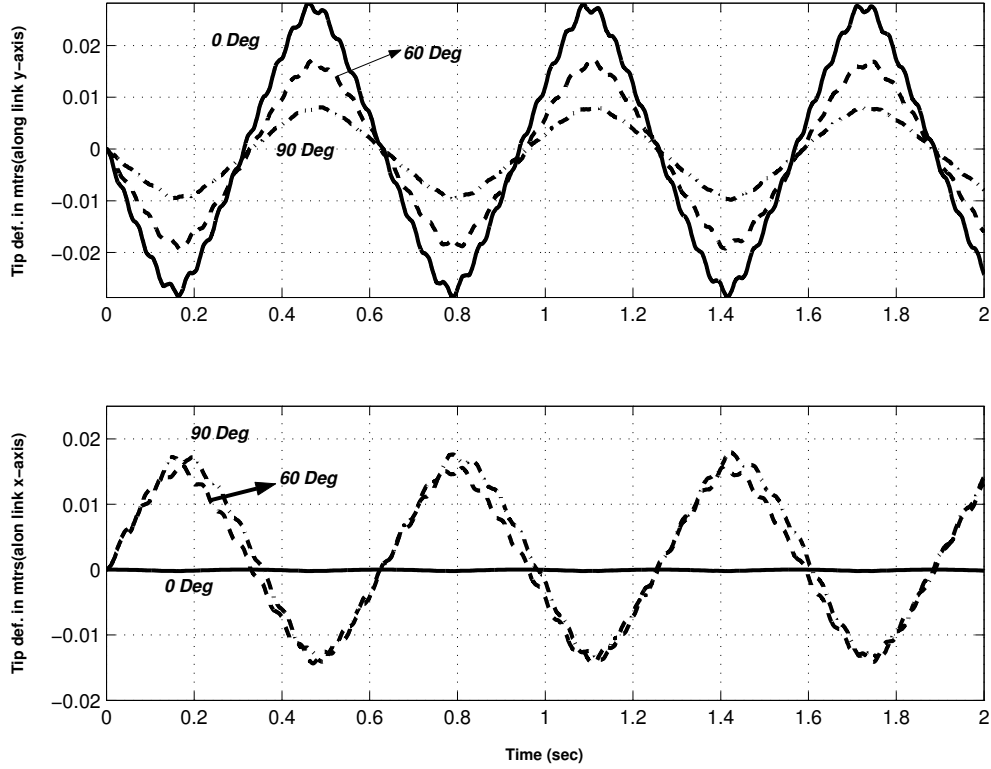
link length=2 m, $\rho A = 0.1 kg/m$, $\tau = 5\sin(1t)$, $\delta = 0\deg$, $U_a = 4800m/sec$

Figure 10: (a) Plot of first natural frequency vs time   (b) Plot of first natural frequency vs U_g

length of the link decreases thereby increasing the flexural stiffness of the link. However, the tip deflection along the X-axis of the link co-ordinate system, as shown in bottom half of figure 11, increases till the kink angle reaches 90 deg and then decreases as the kink angle

18

further increases.

link length=2 m($L_1 = 1m$, $L_2 = 1m$), $U_g = 25m/sec$, $U_a = 4800m/sec$, $\rho A = 0.1kg/m$, $\tau_1 = 5\sin(10t)$ $N - m$

Figure 11: Tip deflection(along the link Y and X-axis) of 1R kinked manipulator for different kink angles

The significance of nonlinear modeling lies in its accuracy compared to the linear model. The top part of figure 12 shows tip deflection along Y-axis for the linear and nonlinear model of 1R planar kinked manipulator with kink angle 0 deg. The bottom part of figure 12 shows the difference between the linear and nonlinear model and one can observe that the maximum difference is approximately 25 %. Similarly, it was found that for kink angles of 60 deg and 90 deg the linear model shows a maximum difference of approximately 24 % and 23 % compared to the nonlinear model. The differences are clearly significant.

5.4 Comparison of component mode and system mode methods

In the section 4, the finite element based system mode method of modeling a multi-link flexible manipulators was proposed. We compare the simulation results of the finite element based component mode and system mode methods of modeling for the case of a planar 2R flexible manipulator. In the former it was assumed that each individual link of the 2R

19
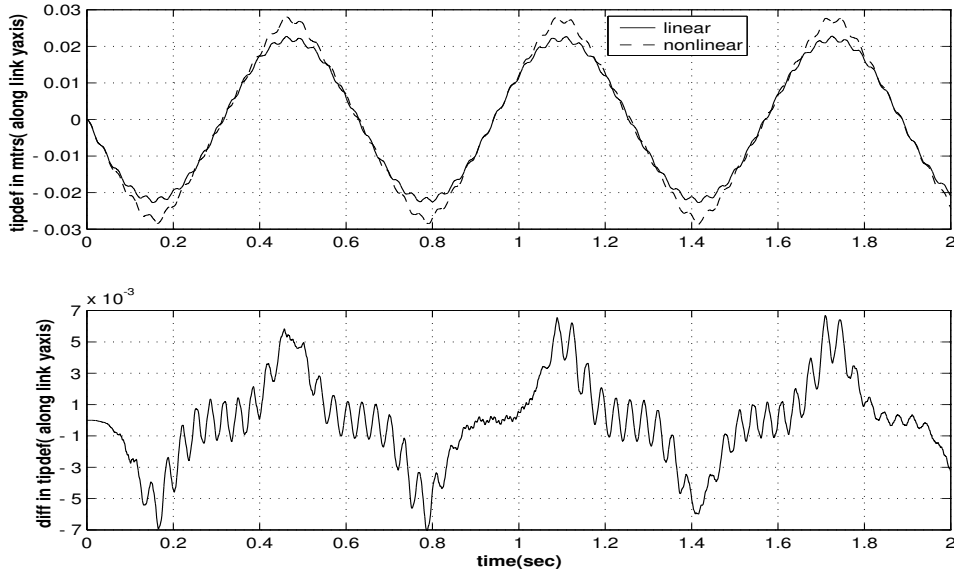
link length=2 m, $U_g = 25m/sec$, $U_a = 4800m/sec$, $\rho A = 0.1kg/m$, $\delta = 0 \deg$,
$$\tau_1 = 5\sin(10t) \ N - m$$

Figure 12: Comparison between linear and nonlinear kinked manipulator with 0 deg kink angle

manipulator vibrates in its component modes with component natural frequencies. In the later, the 2R manipulator vibrates in its system modes with system frequencies. Implicit in the later formulation is the assumption that the second joint is locked at each instant of time. In the modeling of 2R manipulator, using component mode method, *each link* is discretised into two finite elements, i.e., we have in all 4 elements. In the case of the system mode method the *whole system* is discretised into two elements. The time history of the rigid variables(θ_1 and θ_2) for two different flexibilities (corresponding to $U_{g_1} = U_{g_2} = 100$ m/sec and $U_{g_1} = U_{g_2} = 40$ m/sec) are shown in figure 13 and figure 15. It can be observed that when the links are more flexible, the time history of the rigid variables shown by the component mode method deviates from those obtained from the system mode method.

From FEM simulation, it was found that the tip deflection for $U_g = 100$ m/sec, the magnitude of the maximum tip deflection was 10^{-3} for link 1 and 1.5×10^{-4} in link 2. For $U_g = 40$ m/sec, the magnitude of the maximum tip deflection was approximately 7×10^{-3} in link 1 and 2×10^{-3} in link 2. Figure 14 and 16 shows the difference in tip deflections, between system mode and component mode, in link 1 and 2 for U_g values of 100 m/sec and 40 m/sec respectively, with all other quantities remaining same. It can be observed from figure 16, that when U_g of links is smaller the difference in transverse tip deflection is of the order of 10^{-3} whereas when U_g is larger, as in Figure 14, the difference in tip transverse deflection is of the order of 10^{-5}.

From extensive simulation, it was found that the system mode method, for higher U_g values, gives similar behavior as that of the component mode method in terms of joint

20

Modeling method	U_{g_1}=100 m/sec U_{g_2}=100 m/sec	U_{g_1} = 40 m/sec U_{g_2} = 40 m/sec
System mode	147.82 sec	2723.70 sec
Component mode	903.85 sec	6468.5 sec

Table 1: Simulation time for component mode and system mode methods

rotation and tip displacements with fewer number of elements. A representative case, figure 13 shows plot of θ_1 and θ_2 versus time for component mode and system mode approaches with four elements taken for component mode and two elements for system mode. As a consequence of less number of finite elements in system mode method approach, the number of ordinary differential equations is also less, and this is reflected in the considerably reduced computational time as shown in Table 1.
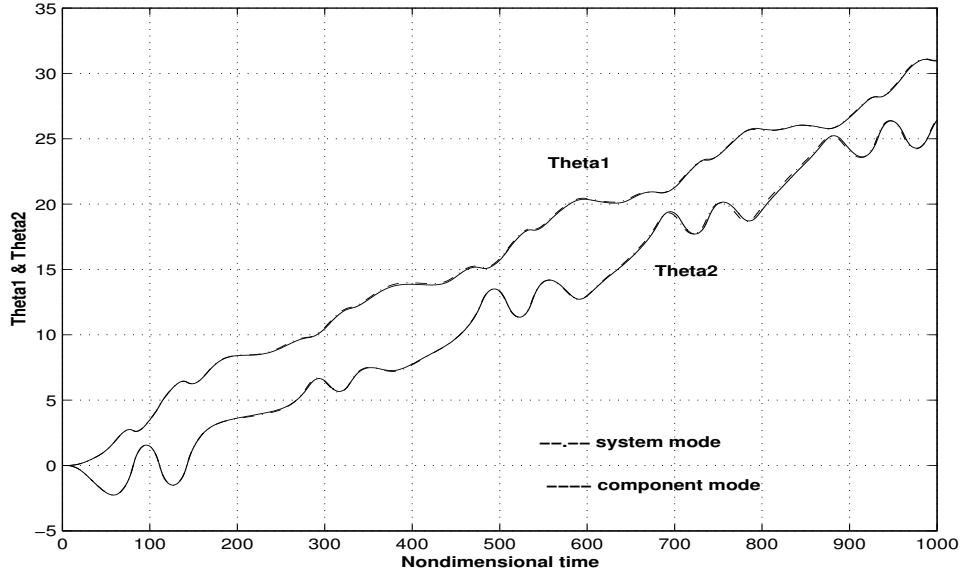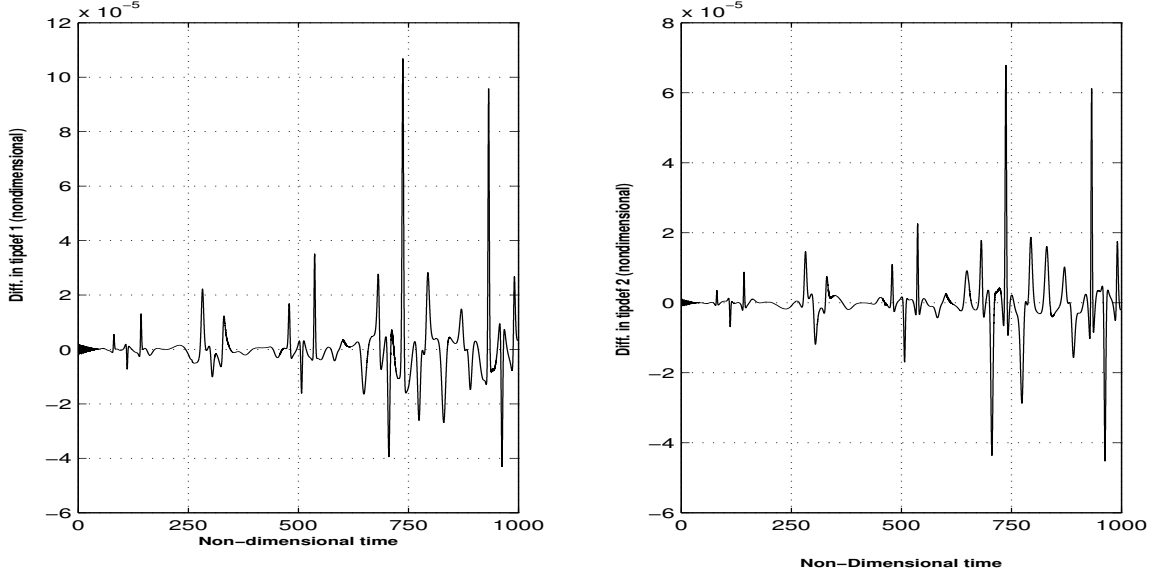

link1=1 m, link2=1 m, $U_{g_1} = 100m/sec$, $U_{a_1} = 4800m/sec$, $U_{g_2} = 100m/sec$, $U_{a_2} = 4800m/sec$, $\rho_1 A_1 = 0.1kg/m$, $\rho_2 A_2 = 0.1kg/m$, $\tau_1 = 2\sin(3t)\ N-m$, $\tau_2 = 0\sin(0t)\ N-m$

Figure 13: Plot of θ_1 and θ_2 versus non-dimensional time for component mode and system mode methods

6 Conclusions

This paper deals with non-linear models, derived from a non-linear strain-displacement relationship, of planar flexible manipulators with one and two revolute joints. The non-linear
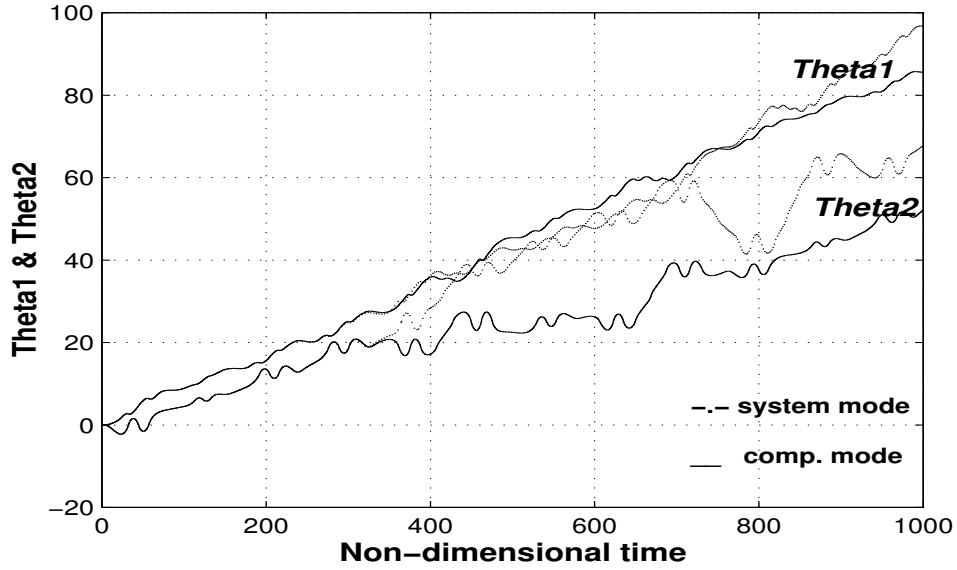
$$\text{link1=1 m, link2=1 m, } U_{g_1} = 100m/sec, \ U_{a_1} = 4800m/sec, \ U_{g_2} = 100m/sec,$$
$$U_{a_2} = 4800m/sec, \ \rho_1 A_1 = 0.1kg/m, \ \rho_2 A_2 = 0.1kg/m,$$
$$\tau_1 = 2\sin(3t) \ N - m, \tau_2 = 0\sin(0t) \ N - m$$

Figure 14: Comparison of FEM based component mode and system mode methods of modeling 2R planar manipulator

finite element mathematical models for flexible manipulator systems and the Lagrangian formulation was used to derive the equations of motion of the systems. An algorithm for the non-dimensionalisation of the equations of motion based on two characteristic velocities, representing the flexural and axial rigidity of flexible links, was developed. A finite element based system mode method of modeling the multi-link flexible manipulators has been developed and is compared with the conventional component mode method. As a pre-requisite to the system mode method of modeling a two-link flexible manipulator, a study of dynamics of single link kinked manipulator has been conducted. Extensive numerical simulation of the above mentioned models lead to the following main conclusions:

- The tip deflection obtained from linear and nonlinear models are significantly different when the actuating torque frequency is low. The difference becomes small when the actuation torque frequency is increased. Hence nonlinear models are more relevant for low actuation frequencies.

- The proposed kinked beam method of modeling flexible manipulators was found to give significantly different results compared to the conventional modeling technique at low actuation frequencies of the joint torque. At high actuation frequencies of the torque or large flexural stiffness of the links there is not much variation in the tip deflection shown by both methods.

22

link1=1 m, link2=1 m, $U_{g_1} = 40m/sec$, $U_{a_1} = 4800m/sec$, $U_{g_2} = 40m/sec$,
$U_{a_2} = 4800m/sec$, $\rho_1 A_1 = 0.1 kg/m$, $\rho_2 A_2 = 0.1 kg/m$,
$\tau_1 = 2\sin(3t)$ $N - m$, $\tau_2 = 0\sin(0t)$ $N - m$

Figure 15: Plot of θ_1 and θ_2 versus non-dimensional time for component mode and system mode methods

- The comparison of linear and nonlinear models of 1R planar flexible manipulator indicates that above a certain flexural rigidity (corresponding to U_g approximately ≥ 45 m/sec), the linear and non-linear model show almost same tip deflection. Hence, non-linear models should be employed only if flexural rigidities of the links are low.

- The flexural rigidity is seen to be dominating the axial rigidity. At high flexural rigidity values the axial elongation or tip transverse deflection remain small and almost constant irrespective of the axial rigidity. The effect of axial rigidity shows up only at low flexural rigidity of links.

- The tip deflection along the Y-axis of the link co-ordinate system of the 1R kinked manipulator is seen to be decreasing with the increase in the kink angle. This is because the effective length of the link decreases thereby increasing the flexural stiffness of the kinked link.

- The study of the effect of U_a and U_g on dynamics of 1R planar flexible manipulator revealed that the natural frequencies vary non-linearly with U_a and in a linear fashion with U_g.

- As the links of multi-link flexible manipulators become more and more flexible(U_g is made smaller), the component mode method of modeling shows greater deviation
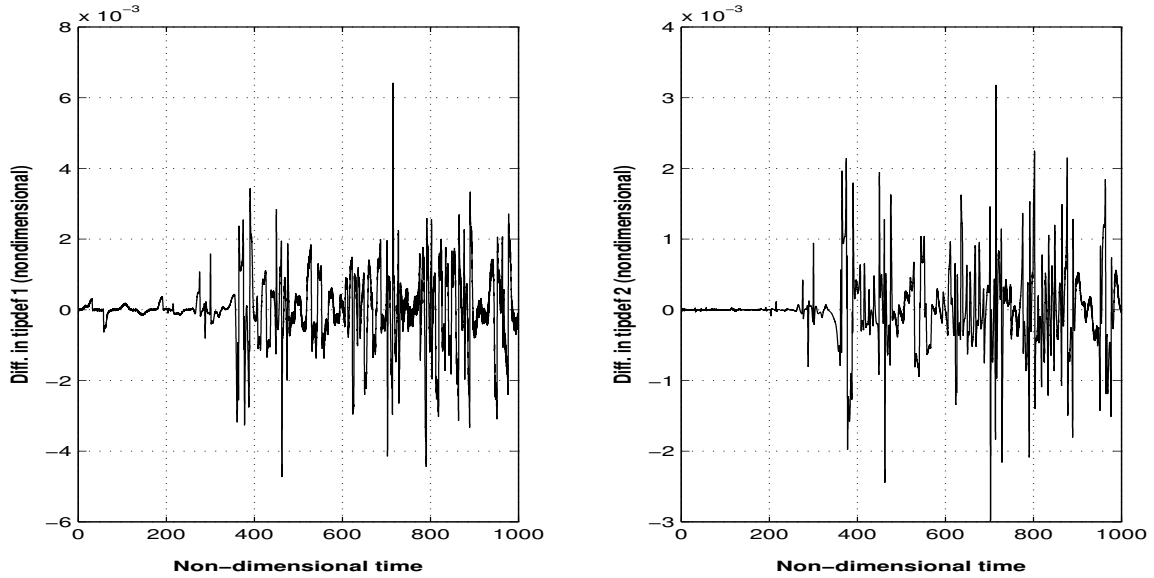
23

link1=1 m, link2=1 m, $U_{g_1} = 40 m/sec$, $U_{a_1} = 4800 m/sec$, $U_{g_2} = 40 m/sec$,
$U_{a_2} = 4800 m/sec$, $\rho_1 A_1 = 0.1 kg/m$, $\rho_2 A_2 = 0.1 kg/m$,
$\tau_1 = 2 \sin(3t) \ N - m, \tau_2 = 0 \sin(0t) \ N - m$

Figure 16: Comparison of FEM based component mode and system mode methods of modeling 2R planar manipulator

from the system mode method. For high values of U_g there is almost no difference in behavior in terms of tip deflection and joint rotation. In addition, the computation time for system mode approach is significantly less than the component mode method because of the reduction in number of ordinary differential equations to be numerically integrated. Hence, for high U_g values, the system mode formulation yields system behavior significantly faster than a traditional component mode formulation with very little difference from the traditional component mode formulation.

Acknowledgements

References

[1] Bahgat, B. M and Willmert, K. D, 1976, "Finite Element Vibration Analysis of Planar Mechanisms", *Mechanisms and Machines Theory*, Vol. 11, pp. 47-71.

[2] Midha, A., Erdman, A. G. and Frohib, D. A., 1978, "Finite Element Approach to Mathematical Modeling of High Speed Elastic Linkages", *Mechanisms and Machines Theory*, Vol. 13, pp. 603-618.

[3] Book, W. J., 1984, "Recursive Lagrangian Dynamics of Flexible Manipulator Arms", *The International Journal of Robotics Research*, Vol. 3(3), pp. 87-101.

[4] Hastings, G. and Book, W. J., 1987, "Linear Dynamic Model for Flexible Link Manipulator", *IEEE Control System Magazine*, Vol. 7(1), pp. 61-64.

[5] Trucic, D. A. and Midha, A., 1984, "Generalized Equations of Motion for Dynamic Analysis of Elastic Mechanism", ASME *Journal of Dynamic Systems, Measurement and Control*, Vol. 106, pp. 243-248.

[6] Usoro, P. B., Nadira, R. and Mahil, S. S., 1986, "A Finite Element Lagrange Approach to Modeling Light Weight Flexible Manipulators", ASME *Journal of Dynamic Systems, Measurements and Control*, Vol. 108, pp. 198-205.

[7] Nagaraj, B. P., Nataraju, B. S. and Ghosal, A., 1997, "Dynamics of a Two-link Flexible System Undergoing Locking: Mathematical Modeling And Comparisons With Experiments", *Journal of Sound and Vibration*, Vol. 207(4), pp. 567-589.

[8] Theodore, R. J. and Ghosal, A., 1995, "Comparison of Assumed Mode and Finite Element Methods for Flexible Multi-link Manipulators", *The International Journal of Robotics Research*, Vol. 14(2), pp. 91-111.

[9] Przemieniecki, J. S., 1968, *Theory of Matrix Structural Analysis*, McGraw-Hill Book Co.

[10] Bakr, E. M. and Shabana, A. A., 1986, "Geometrically Non-linear Analysis of Multibody systems", *Computers and Structures*, Vol. 23(6), pp. 739-751.

[11] Gordaninejad, F., Azhdari, A. and Chalhoub, N. G., 1989, "The Combined Effects of Geometric Non-linearity and Shear Deformation on the Performance of a Revolute-Prismatic Flexible Composite-Material Robot Arm", *Proceedings of the Fourth International Conference on CAD, CAM, Robotics and Factories of the Future*, Indian Institute of Technology, New Delhi, Dec. 19-22, Vol. 1, pp. 620-638.

[12] Damaren, C., and Sharf, L., 1995, "Simulation of Flexible-Link Manipulators with Inertia and Geometric Nonlinearities", *ASME J of Dynamic, Systems, Measurement and Control*, Vol. 117 pp., 74-87.

[13] Simo, J.C., and Vu-Quoc, L., 1987, "The Role of Nonlinear Theories in Transient Dynamic Analysis of Flexible Structures", *Journal of Sound and Vibration*, Vol. 119(3), pp. 487-508.

25

[14] Mayo, J., Dominguez, J. and Shabana, A. A., 1995, "Geometrically Nonlinear Formulations of Beams in Flexible Multi-body Dynamics", *Journal of Vibration and Acoustics*, Vol. 117, pp. 501-509.

[15] Absy, H. EL and Shabana, A. A., 1997, "Geometric stiffness and stability of rigid body modes", *Journal of Sound and Vibration*, Vol. 207(4), pp. 465-496.

[16] Du, H. and Ling, S. F., 1995, "A Nonlinear Dynamic Model for Three-Dimensional Flexible Linkages", *Computers and Structures*, Vol. 56(1), pp. 15-23.

[17] Al-Bedoor, B. O. and Hamdan, M. N., 2001, "Geometrically Non-linear Dynamic Model of a Rotating Flexible Arm", *Journal of Sound and Vibration*, Vol. 240(1), pp. 59-72.

[18] Gürgoże M., 1998, "On the Dynamic Analysis of a Flexible L-Shaped Structure", *Journal of Sound and Vibration*, Vol. 211(4), pp. 683-688.

[19] Oguamanam, D. C. D., Hansen, J. S. and Heppler, G. R., 1998, "Vibration of Arbitrarily Oriented Two-Member Open Frames With Tip Mass", *Journal of Sound and Vibration*, Vol. 209(4), pp. 651-669.

[20] Milford, R. I. and Ashokanthan, S. F., 1999, "Configuration Dependent Eigenfrequencies for a Two-link Flexible Manipulator: Experimental Verification", *Journal of Sound and Vibration*, Vol. 222(2), pp. 191-207.

[21] Reddy, B. S., Simha, K. R. Y. and Ghosal, A., 1999., "Free Vibration of a Kinked Cantilever With Attached Masses", *Journal of the Acoustical Society of America*, Vol. 105(1), pp. 164-174.

[22] Agrawal, O. P. and Shabana, A. A., "Dynamic analysis of multi-body systems using component modes", *Computers & Structures*, Vol. 21(6), pp. 1303-1312, 1985.

[23] Witham, G. B., 1986, *Linear and Nonlinear Waves*, John Wiley, New York.

[24] *Matlab Users Manual*, 1994, The MathWorks Inc.

[25] Wolfram, S., 1996, *The Mathematica Book*, 3rd Edition, Cambridge University Press.

Appendix A

In this appendix we present the detailed mass matrix, conventional stiffness matrix, geometric stiffness matrix in their non-dimensional form for the *1R planar kinked manipulator* with kink angle of δ. The mass and stiffness matrices are symmetric and hence only the upper triangular part is presented. In addition, only the non-zero elements of the stiffness matrices are given.

Elements of mass matrix

$$
\begin{aligned}
M(1,1) \;=\;& 1/3 + Lm + (1/3)L^3m + L^2m\cos(\delta+\phi_2) + (2/3)U_2 + 2LmU_2 + L^2m\cos(\delta+\phi_2)U_2 \\
& + (1/3)U_2{}^2 + LmU_2{}^2 + (2/3)L^2mU_4 + Lm\cos(\delta+\phi_2)U_4 + Lm\cos(\delta+\phi_2)U_2U_4 \\
& + (1/3)LmU_4{}^2 + L^2m\sin(\delta+\phi_2)V_2 + Lm\sin(\delta+\phi_2)U_4V_2 + (13/35)V_2{}^2 \\
& + LmV_2{}^2 - Lm\sin(\delta+\phi_2)V_4 - Lm\sin(\delta+\phi_2)U_2V_4 + Lm\cos(\delta+\phi_2)V_2V_4 \\
& + (13/35)LmV_4{}^2 - \frac{11}{105}V_2\phi_2 + (1/105)\phi_2{}^2 + (1/6)L^2m\sin(\delta+\phi_2)\phi_4 \\
& + (1/6)L^2m\sin(\delta+\phi_2)U_2\phi_4 - (1/6)L^2m\cos(\delta+\phi_2)V_2\phi_4 - (11/105)L^2mV_4\phi_4 \\
& + (1/105)L^3m\phi_4{}^2 \\[4pt]
M(1,2) \;=\;& -(1/2)\left(L^2m\sin(\delta+\phi_2)\right) - (1/2)Lm\sin(\delta+\phi_2)U_4 - (7/20)V_2 - LmV_2 \\
& - (1/2)Lm\cos(\delta+\phi_2)V_4 + (1/20)\phi_2 + (1/12)L^2m\cos(\delta+\phi_2)\phi_4 \\[4pt]
M(1,3) \;=\;& 7/20 + Lm + (1/2)L^2m\cos(\delta+\phi_2) + (7/20)U_2 + LmU_2 \\
& + (1/2)Lm\cos(\delta+\phi_2)U_4 - (1/2)Lm\sin(\delta+\phi_2)V_4 + (1/12)L^2m\sin(\delta+\phi_2)\phi_4 \\[4pt]
M(1,4) \;=\;& -1/20 + (1/3)L^3m + (1/2)L^2m\cos(\delta+\phi_2) - (1/20)U_2 + (1/2)L^2m\cos(\delta+\phi_2)U_2 \\
& + (2/3)L^2mU_4 + (1/2)Lm\cos(\delta+\phi_2)U_4 + (1/2)Lm\cos(\delta+\phi_2)U_2U_4 + \frac{1}{3}LmU_4{}^2 \\
& + (1/2)L^2m\sin(\delta+\phi_2)V_2 + (1/2)Lm\sin(\delta+\phi_2)U_4V_2 - (1/2)Lm\sin(\delta+\phi_2)V_4 \\
& - (1/2)Lm\sin(\delta+\phi_2)U_2V_4 + (1/2)Lm\cos(\delta+\phi_2)V_2V_4 + (1/12)L^2m\sin(\delta+\phi_2)\phi_4 \\
& + (13/35)LmV_4{}^2 + (1/12)L^2m\sin(\delta+\phi_2)U_2\phi_4 - (1/12)L^2m\cos(\delta+\phi_2)V_2\phi_4 \\
& - (11/105)L^2mV_4\phi_4 + (1/105)L^3m\phi_4{}^2 \\[4pt]
M(1,5) \;=\;& (1/2)Lm(\sin(\delta+\phi_2) + \sin(\delta+\phi_2)U_2 - \cos(\delta+\phi_2)V_2 - (7/10)V_4 + (1/10)L\phi_4) \\[4pt]
M(1,6) \;=\;& (1/2)Lm(\frac{7}{10}L + \cos(\delta+\phi_2) + \cos(\delta+\phi_2)U_2 + (7/10)U_4 + \sin(\delta+\phi_2)V_2) \\[4pt]
M(1,7) \;=\;& -(1/20)L^3m - (1/12)L^2m\cos(\delta+\phi_2) - (1/12)L^2m\cos(\delta+\phi_2)U_2 \\
& - (1/20)L^2mU_4 - (1/12)L^2m\sin(\delta+\phi_2)V_2 \\[4pt]
M(2,2) \;=\;& 1/3 + Lm, \quad M(2,3) = 0 \\[4pt]
M(2,4) \;=\;& -(1/2)Lm(L\sin(\delta+\phi_2) + \sin(\delta+\phi_2)U_4 + \cos(\delta+\phi_2)V_4 - (1/6)L\cos(\delta+\phi_2)\phi_4) \\[4pt]
M(2,5) \;=\;& (1/2)Lm\cos(\delta+\phi_2), \;\; M(2,6) = -(1/2)Lm\sin(\delta+\phi_2) \\[4pt]
M(2,7) \;=\;& (1/12)L^2m\sin(\delta+\phi_2), \;\; M(3,3) = 13/35 + Lm \\[4pt]
M(3,4) \;=\;& -11/210 + (1/2)L^2m\cos(\delta+\phi_2) + (1/2)Lm\cos(\delta+\phi_2)U_4 \\
& - (1/2)Lm\sin(\delta+\phi_2)V_4 + (1/12)L^2m\sin(\delta+\phi_2)\phi_4 \\[4pt]
M(3,5) \;=\;& (1/2)Lm\sin(\delta+\phi_2), \;\; M(3,6) = (1/2)Lm\cos(\delta+\phi_2) \\[4pt]
M(3,7) \;=\;& -(1/12)L^2m\cos(\delta+\phi_2) \\[4pt]
M(4,4) \;=\;& 1/105 + (1/3)L^3m + (2/3)L^2mU_4 + (1/3)LmU_4{}^2 + (13/35)LmV_4{}^2 \\
& - (11/105)L^2mV_4\phi_4 + (1/105)L^3m\phi_4{}^2 \\[4pt]
M(4,5) \;=\;& -(7/20)LmV_4 + (1/20)L^2m\phi_4, \quad M(4,6) = (7/20)L^2m + (7/20)LmU_4
\end{aligned}
$$

$$M(4,7) = -(1/20)L^3m - (1/20)L^2mU_4, \quad M(5,5) = (1/3)Lm, \quad M(5,6) = M(5,7) = 0$$
$$M(6,6) = (13/35)Lm, \quad M(6,7) = -(11/210)L^2m, \quad M(7,7) = (1/105)L^3m$$

Linear stiffness matrix

The non-zero elements of $[\mathcal{K}]$ are:

$$\mathcal{K}(3,3) = 12, \quad \mathcal{K}(3,4) = -6, \quad \mathcal{K}(4,4) = 4$$
$$\mathcal{K}(6,6) = \frac{12mU_{g_2}^2}{LU_{g_1}^2}, \quad \mathcal{K}(6,7) = \frac{-6mU_{g_2}^2}{U_{g_1}^2}, \quad \mathcal{K}(7,7) = \frac{4LmU_{g_2}^2}{U_{g_1}^2}$$

Elements of geometric stiffness matrix

$$\Delta\mathcal{K}(2,2) = (U_{a_1}/U_{g_1})^2, \quad \Delta\mathcal{K}(2,3) = (U_{a_1}/U_{g_1})^2\left((3/5)V_2 - (1/20)\ \phi_2\right)$$
$$\Delta\mathcal{K}(2,4) = -(U_{a_1}/U_{g_1})^2((1/20)\ V_2 + (1/15)\ \phi_2)$$
$$\Delta\mathcal{K}(3,3) = (U_{a_1}/U_{g_1})^2\ (3/5)U_2, \quad \Delta\mathcal{K}(3,4) = -(U_{a_1}/U_{g_1})^2\ (1/20)U_2$$
$$\Delta\mathcal{K}(4,4) = (U_{a_1}/U_{g_1})^2\ ((1/15)U_2), \quad \Delta\mathcal{K}(5,5) = (U_{a_2}/U_{g_1})^2\ (m/L)$$
$$\Delta\mathcal{K}(5,6) = (U_{a_2}U_{g_1})^2\ ((3/5)\ (m/L^2)V_4 - (1/20)\ (m/L)\phi_4)$$
$$\Delta\mathcal{K}(5,7) = -(U_{a_2}/U_{g_1})^2\ ((1/20)\ (m/L)V_4 + (1/15)\ m\phi_4)$$
$$\Delta\mathcal{K}(6,6) = (U_{a_2}U_{g_1})^2\ ((3/5)\ (m/L^2)U_4), \quad \Delta\mathcal{K}(6,7) = -(U_{a_2}/U_{g_1})^2\ ((1/20)(m/L)U_4)$$
$$\Delta\mathcal{K}(7,7) = (U_{a_2}/U_{g_1})^2\ ((1/15)\ mU_4)$$

Appendix B

In this appendix, we derive the position vector of the tip of a planar single link manipulator modeled using the conventional[6, 8] and our proposed method. In both cases, the link is assumed to be discretised into two elements.

Proposed Approach

The position vector of an arbitrary point in the first element, as shown in figure 17, is given by,

$$_1^0\mathbf{P} = [R_{\theta 1}]\left\{\begin{array}{c} x + u_{x_1} \\ u_{y_1} \end{array}\right\} \qquad 0 \leq x \leq L_1$$

Similarly, the position vector of an arbitrary point in the second element is given by

$$_2^0\mathbf{P} = \left._1^0\mathbf{P}\right|_{x=L_1} + \left[R_{(\theta_1+\phi_2)}\right]\left\{\begin{array}{c} x + u_{x_2} \\ u_{y_2} \end{array}\right\} \qquad 0 \leq x \leq L_2$$
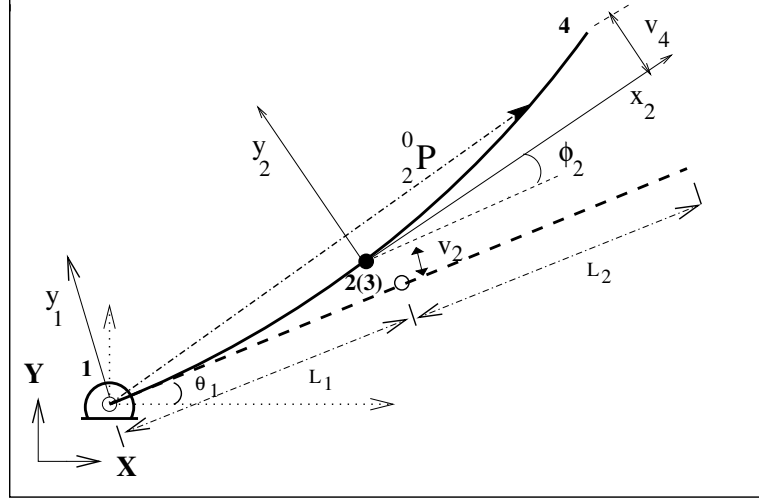
Figure 17: Single link planar manipulator(Proposed approach)

where,

$$\left\{ \begin{array}{c} u_{x_1} \\ u_{y_1} \end{array} \right\} = f(u_1, v_1, \phi_1, u_2, v_2, \phi_2), \left\{ \begin{array}{c} u_{x_2} \\ u_{y_2} \end{array} \right\} = f(u_3, v_3, \phi_3, u_4, v_4, \phi_4)$$

and $\{q_i\} = \{u_{2i-1}, v_{2i-1}, \phi_{2i-1}, u_{2i}, v_{2i}, \phi_{2i}\}$ is the vector of the nodal variables of the ith element in its local co-ordinate system. From the above, the position vector of the tip of the link is given by

$$\left. {}^0_2\mathbf{P} \right|_{x=L_2} = [R_{\theta 1}] \left\{ \begin{array}{c} L_1 + u_2 \\ v_2 \end{array} \right\} + [R_{\theta 1}] \left[R_{\phi 2} \right] \left\{ \begin{array}{c} L_2 + u_4 \\ v_4 \end{array} \right\}$$

$$= [R_{\theta 1}] \left(\left\{ \begin{array}{c} L_1 \\ 0 \end{array} \right\} + [R_{\phi 2}] \left\{ \begin{array}{c} L_2 \\ 0 \end{array} \right\} \right) + [R_{\theta 1}] \left(\left\{ \begin{array}{c} u_2 \\ v_2 \end{array} \right\} + [R_{\phi 2}] \left\{ \begin{array}{c} u_4 \\ v_4 \end{array} \right\} \right) \quad (22)$$

Conventional Approach

In the conventional approach [6, 7, 8], the position vector of an arbitrary point in second element, shown in figure 18, is given by

$$ {}^0_2\mathbf{P} = \left[R_{(\theta_1)} \right] \left\{ \begin{array}{c} L_1 + x + u_{x_2} \\ u_{y_2} \end{array} \right\} \qquad 0 \leq x \leq L_2 $$

where,

$$\left\{ \begin{array}{c} u_{x_1} \\ u_{y_1} \end{array} \right\} = f(u_1, v_1, \phi_1, u_2, v_2, \phi_2), \left\{ \begin{array}{c} u_{x_2} \\ u_{y_2} \end{array} \right\} = f(u_2, v_2, \phi_2, u_3, v_3, \phi_3)$$

and $\{q_i\} = \{u_i, v_i, \phi_i, u_{i+1}, v_{i+1}, \phi_{i+1}\}$ is the vector of the nodal variables of the ith element in the global co-ordinate system. Therefore, the position vector of the tip of the link can be obtained as,
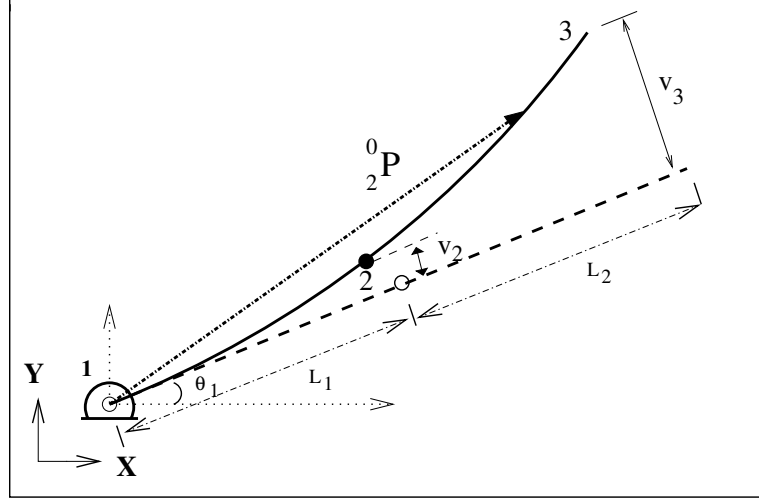
Figure 18: Single link planar manipulator(Conventional approach)

$$
\left. {}_2^0\mathbf{P} \right|_{x=L_2} = [R_{\theta 1}] \left(\left\{ \begin{array}{c} L_1 \\ 0 \end{array} \right\} + \left\{ \begin{array}{c} L_2 \\ 0 \end{array} \right\} \right) + [R_{\theta 1}] \left\{ \begin{array}{c} u_3 \\ v_3 \end{array} \right\} \tag{23}
$$

The difference between the proposed approach and the conventional approach is seen from the last term in equations (23) and (22). In equation (22), there is an additional term $[R_{\phi_2}](u_4, v_4)^T$ which represent the coupling between the rotation at the second node and subsequent elements. This term is not present in equation (23). Since the position vectors are different from the conventional approach, the elements of the mass matrix, derived from the position vector, are different in the proposed approach.